GEORGE BROWN PRESS
JOURNALS, BOOKS & PROCEEDINGS

International Journal of Engineering Advances

Article

Design of a Laser Beam Pointing Stabilization System Based on Dual-Level Feedback for 4-Axis PZT Interlock Control

Jinqiang Chen [1,*]

[1] Songshan Lake Materials Laboratory, Dongguan, China
* Correspondence: Jinqiang Chen, Songshan Lake Materials Laboratory, Dongguan, China

Abstract: To enhance the pointing stability of laser beams in precision optical systems, this study develops a four-axis piezoelectric (PZT)-driven interlinked control architecture equipped with a dual-stage feedback mechanism. The system is designed to suppress multi-axis disturbances that typically degrade beam alignment accuracy in high-frequency operational environments. A coupled mathematical model describing the dynamic interaction between the laser beam and mirror frame is established, forming the foundation for precise motion control analysis. Based on this model, an inverse matrix decoupling algorithm is integrated to compensate for cross-axis coupling effects, thereby enabling real-time fine-tuning of each control channel. The system's dynamic response characteristics are comprehensively analyzed through both simulation and experimental validation, focusing on tracking accuracy, frequency response, and long-term drift behavior. Experimental results indicate that the proposed control system maintains sub-micron beam stability even under high-frequency and multi-directional disturbances. The control loop demonstrates excellent repeatability, minimal overshoot, and strong immunity to environmental vibration and thermal fluctuation. Compared with conventional single-axis or uncoupled PZT control methods, the proposed interlinked configuration exhibits faster convergence, higher positioning precision, and improved disturbance rejection capability. These advantages confirm that the developed system meets the stringent requirements of advanced laser applications, such as beam steering, optical communication alignment, and high-precision material processing in complex operational conditions. The research provides a reliable reference for designing multi-axis active stabilization systems in next-generation high-performance laser platforms.

Keywords: beam stabilization; PZT control; decoupling algorithm; system modeling; experimental validation

Received: 14 October 2025
Revised: 26 October 2025
Accepted: 08 November 2025
Published: 12 November 2025

1. Introduction

High-precision laser systems play a critical role in fields such as optical communication, precision metrology, inertial navigation, and laser-based manufacturing. In these applications, the pointing stability of the laser beam directly determines the system's accuracy, energy efficiency, and long-term reliability. Minor angular deviations or displacement errors can lead to significant optical misalignment, signal attenuation, or reduced measurement precision, particularly under dynamic or high-frequency operational conditions.

Conventional single-loop or independent-axis control architectures often fail to provide sufficient compensation when subjected to multi-axis coupled disturbances, high-frequency vibrations, or environmental fluctuations. These systems typically exhibit dynamic drift, overshoot, and limited long-term stability due to their restricted bandwidth and inability to coordinate control across multiple axes. To address these limitations, it is essential to integrate multi-axis sensing, fast actuation, and advanced control algorithms, enabling coordinated compensation for all degrees of freedom.

To meet these requirements, this study develops a four-axis PZT-based interlinked control system with a dual-stage feedback structure. The system achieves precise regulation of both angular orientation and linear displacement, mitigating the adverse effects of cross-axis coupling and environmental disturbances [1]. The research covers the complete design process, including system-level architecture planning, hardware configuration, dynamic modeling, and the development of a decoupling algorithm based on inverse matrix principles.

Experimental validation is conducted to evaluate the system's dynamic response, steady-state behavior, and long-term stability. Results demonstrate that the control approach provides high pointing accuracy, rapid disturbance rejection, and strong immunity to external vibration and thermal drift. The proposed solution establishes a reliable framework for beam pointing stabilization in high-precision optical systems operating under complex and challenging conditions, offering practical guidance for the design of next-generation laser platforms with stringent performance requirements.

2. Overall Design of the Beam Stabilization System

The overall design of the beam stabilization system is focused on achieving high-precision pointing control under complex operational conditions. The system integrates a three-layer synergy of optics, mechanics, and control to suppress disturbances and maintain the long-term stability of the optical axis. To address the different frequency characteristics of environmental perturbations, the system employs a fast-slow dual-channel feedback strategy. The fast loop is responsible for mitigating high-frequency perturbations by driving mirrors with high-response PZT actuators, providing rapid angular corrections to maintain instantaneous beam alignment. Meanwhile, the slow loop addresses low-frequency drift, utilizing high-precision position sensor modules to detect displacement errors and generate compensation signals for long-term steady-state correction [2].

The optical-mechanical structure is designed with a rigid-flexible coupling layout to balance structural rigidity with vibration damping. This configuration effectively reduces mechanical resonance effects on the optical axis while preserving sufficient compliance to absorb minor vibrations without introducing excessive stress to the mirrors or actuators. In addition, careful placement of mirrors, mounts, and sensor modules minimizes cross-axis interference, ensuring that each axis can respond independently to control signals.

On the electronic control side, decoupling algorithms are implemented to compensate for inter-axis coupling and enhance independent response regulation across all four axes. These algorithms analyze the system's dynamic behavior in real time and adjust control commands to prevent performance degradation due to cross-axis interactions. The modular design of both hardware and software components allows for flexible parameter tuning, channel matching, and iterative optimization, enabling the system to maintain high stability and rapid response even in environments with multi-axis, high-frequency disturbances.

As shown in Figure 1, the overall architecture illustrates the interaction between the optical, mechanical, and electronic layers, as well as the signal flow for dual-stage feedback control in the four-axis PZT-driven beam stabilization system. The design facilitates not only precise beam alignment but also scalability for future enhancements, such as integration with adaptive optics, advanced sensors, or higher-order control loops, providing a robust framework for next-generation precision laser applications.

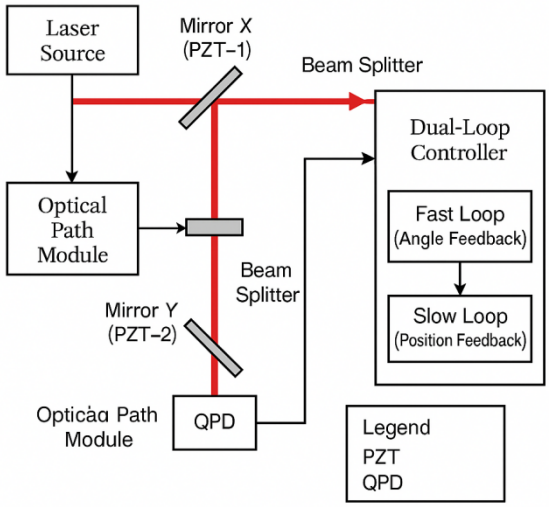

Figure 1. Overall Block Diagram of the Beam Stabilization System.

3. System Hardware Configuration

3.1. Optical Path Layout and Actuators

The optical path of the beam stabilization system employs a two-stage reflective structure to enable independent control across four axes. Following collimation, the laser beam sequentially impinges on the X- and Y-axis mirrors, driven by PZT-1 and PZT-2 actuators, respectively, to perform precise micro-angle adjustments. This configuration simultaneously compensates for disturbances in both planar and pitch directions [3].

Mirror mounts are fabricated from lightweight, high-stiffness materials and incorporate flexible hinges to transmit micro-displacements accurately, ensuring linear angular response even under high-frequency vibrations. The optical path layout is designed according to principles of minimal propagation distance and symmetrical configuration, reducing thermal drift and mechanical coupling errors. Mirror tilt angles are initially set using precision helical adjustment seats, and optical axis stability is verified through interferometer-assisted alignment to ensure sub-micron accuracy.

The actuator system employs a four-channel parallel drive mode, allowing independent control of beam deflection and focal drift. This enables rapid attitude correction and high-resolution modulation of the laser beam under dynamic disturbance conditions. As shown in Figure 2, the schematic illustrates the optical path layout, mirror mounting structure, and the corresponding PZT drive control relationships, highlighting the integration of optics and mechanical actuation for precision stabilization.

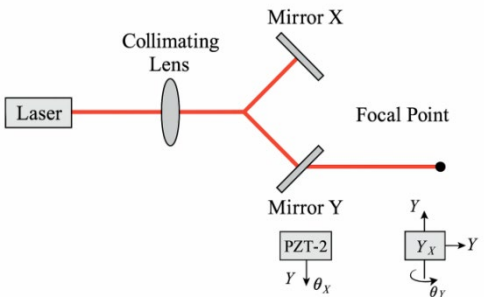

Figure 2. Schematic of optical path layout and mirror mounting structure.

3.2. Position Detection Module

The position detection module functions as the core sensing unit for the dual-stage feedback control system. It captures real-time beam spot displacement and converts it into

error signals for corrective feedback. A high-sensitivity quadrant photodetector (QPD) is employed to measure lateral and longitudinal displacement components by analyzing the energy distribution of the incident light spot [4].

The voltage signals from the detector pass through preamplification and low-noise filtering stages before being fed to the controller. This process suppresses measurement errors arising from background interference, optical power fluctuations, and electronic noise. To further enhance signal linearity and dynamic range, the detection surface undergoes sub-micron-level flatness processing, and the detector is precisely aligned coaxially with the optical axis during installation. A temperature compensation module installed between the QPD and the sampling circuit automatically corrects for drift due to thermal variation. Frequency response testing demonstrates that the detection module achieves an effective bandwidth of several hundred hertz, providing robust real-time data for high-frequency disturbance rejection.

3.3. Piezoelectric Ceramic Drive and Control System

The piezoelectric ceramic (PZT) drive and control system constitutes the primary actuator for precise beam attitude adjustments. High-linearity PZT stacked drivers are employed to achieve nanometer-level displacement resolution through closed-loop voltage control [5]. The drivers interface with a digital signal control board via dedicated amplification modules using differential outputs, minimizing high-frequency noise coupling.

Control voltages are generated by a 16-bit digital-to-analog converter (DAC) and protected with hardware limiting circuits to prevent polarization reversal caused by overvoltage. Embedded strain sensors within the PZT stack provide real-time displacement monitoring, enabling PID parameter self-tuning to optimize the balance between response speed and system stability. The control system also incorporates internal overcurrent and temperature-rise protection logic, ensuring long-term reliability during continuous high-frequency operation. PZT drive signal synchronization across four axes is managed by an FPGA-based timing module, coordinating simultaneous outputs to maintain phase consistency and dynamic precision in mirror attitude adjustments. This configuration ensures that the laser beam remains stable and accurately directed even under complex, multi-axis disturbance conditions.

4. Control System Modeling and Algorithms

4.1. Beam-Mirror Coupling Mathematical Model

The beam-mirror coupling mathematical model establishes the dynamic response relationship between drive voltage and beam deflection. Under PZT drive, the mirror undergoes minute angular displacement around its pivot point. Subject to the combined effects of inertia, damping, and elastic restoring forces, its motion equation can be expressed as:

$$J\ddot{\theta}(t) + B\dot{\theta}(t) + K\theta(t) = k_p V(t) \quad (1)$$

where J is the mirror frame's moment of inertia, B is the viscous damping coefficient, K is the system stiffness, θ(t) is the angular displacement of the mirror surface,k_p is the piezoelectric drive coefficient, and V(t) is the control voltage. Using the small-angle approximation, the beam displacement $\Delta x = 2L\theta(t)$ is obtained, where L is the distance from the mirror to the detection plane. To ensure model accuracy, the system measures the dynamic response of the mirror frame using a step excitation signal during the calibration phase. Parameters J, B, and K are obtained by least-squares fitting. After discretization, the model is input to the controller to achieve dynamic compensation and real-time prediction of high-frequency disturbances.

4.2. Construction and Sampling of System Response Matrix

The system response matrix defines the linear mapping between the four-axis PZT drive voltages and the corresponding beam spot displacement on the detection plane. To accurately determine this response matrix, a small-signal sinusoidal scanning method was employed, independently exciting each PZT axis. Under fixed frequency and amplitude conditions, the output signals from the four-quadrant photodetector were recorded, and steady-state response coefficients were obtained through precise data fitting. By systematically characterizing the influence of each actuator on the measured spot position, the system establishes the following matrix model:

$$\begin{bmatrix}\Delta x\\ \Delta y\end{bmatrix} = \begin{bmatrix}a_{11}a_{12}\\ a_{21}a_{22}\end{bmatrix}\begin{bmatrix}\Delta V_x\\ \Delta V_y\end{bmatrix} \quad (2)$$

where Δx and Δy represent spot displacement (μm), $\Delta V_x, \Delta V_y$ denote X and Y axis control voltages (V), and a_{ij} are the corresponding inter-axis response coefficients. The sampling frequency is set to 10 kHz. After low-pass filtering and normalization, the data is input into the matrix fitting program. To eliminate cross-coupling errors, an axis-by-axis excitation-cross compensation calibration strategy is adopted. Matrix elements are optimized using the least squares algorithm, ultimately yielding a high-precision static response model that provides fundamental parameters for subsequent decoupling control algorithms.

4.3. Decoupling Control Algorithm Based on Inverse Matrix

The inverse matrix-based decoupling control algorithm eliminates cross-interference among the four PZT axes to achieve independent control of spot displacement. The system first invokes the calibrated response matrix A and computes its inverse matrix A^{-1}. This matrix performs the spatial transformation of the control signal:

$$\begin{bmatrix}\Delta V_x\\ \Delta V_y\end{bmatrix} = A^{-1}\begin{bmatrix}E_x\\ E_y\end{bmatrix} \quad (3)$$

Where E_x, E_y represents the normalized error signal from the detector output, and $\Delta V_x, \Delta V_y$ denotes the corresponding PZT drive voltage increment. The algorithm comprises four steps: error acquisition, matrix operations, voltage distribution, and clipping protection. The controller implements matrix inversion in floating-point format within the FPGA, with a 1 kHz update cycle. To enhance numerical stability, LU decomposition is employed for matrix inversion with condition number constraints to prevent drive saturation caused by singular responses. After real-time compensation, the four-axis outputs are synchronously updated via DACs, ensuring independent controllability of beam deflection under multidimensional disturbances.

5. System Testing and Performance Analysis

5.1. Test Platform Setup and Experimental Method

The test platform was constructed to evaluate the system's pointing stability under dynamic disturbance conditions. The experimental setup consisted of a laser source, two-stage mirror assemblies, a quadrant photodetector, PZT drive modules, a control unit, and a high-speed data acquisition system. The entire optical path was mounted on an anti-vibration optical platform to minimize external mechanical interference. After collimation, the laser beam sequentially reflected off the mirrors driven by PZT-1 and PZT-2 before being projected onto the center of the detector, ensuring precise alignment along the optical axis.

The control system, implemented on an FPGA-based main control board, operated with a sampling frequency of 10 kHz and a drive voltage range of ±100 V. Error signals from the detector were acquired through a high-precision analog-to-digital converter (ADC) and processed in real time by the controller to execute closed-loop compensation. To simulate structural vibrations and environmental disturbances, external excitations were applied using a piezoelectric vibration table with a frequency range of 0-300 Hz.

The testing procedure involved multiple sets of repeated experiments. Each set recorded beam spot displacement, corresponding drive voltage responses, and spectral characteristics of the signal. This comprehensive data collection provides the basis for evaluating the system's dynamic performance and quantifying its stability under controlled disturbance conditions.

5.2. Open-Loop Disturbance Characterization

To quantify the system's dynamic response characteristics under varying disturbance intensities and frequencies, open-loop spot displacement tests were conducted. The piezoelectric vibration table applied three levels of disturbance acceleration: 0.1 g, 0.3 g, and 0.5 g, with frequencies ranging from 50 Hz to 600 Hz. Each measurement was repeated three times per condition, and the mean value was taken to reduce experimental uncertainty. After filtering and normalization of the quadrant detector outputs, statistical results of peak spot displacement under different operating conditions were obtained.

As shown in Table 1, the results summarize the peak displacements along the X- and Y-axes, as well as the corresponding phase differences and time delays.

Table 1. Statistics of Peak Spot Displacement under Different Disturbance Conditions.

Disturbance Frequency/ Hz	Disturbance Acceleration (g)	X-axis Peak Displacement (μm)	Y-axis Peak Displacement (μm)	Peak Phase Difference (°)	Peak Time Delay (ms)
50	0.1	2.6	2.4	3.1	1.2
100	0.1	3.2	3.0	5.4	1.4
200	0.3	5.8	5.1	8.7	1.9
300	0.3	8.9	7.6	10.3	2.1
400	0.5	12.4	10.8	13.5	2.4
500	0.5	15.1	13.7	16.8	2.7
600	0.5	18.6	16.9	19.2	3.0

As shown in Table 1, the peak displacement of the optical spot exhibits a nonlinear increase with both disturbance frequency and acceleration. A pronounced resonance response is observed in the 300-500 Hz range, indicating heightened sensitivity to structural and dynamic coupling effects. The Y-axis displacement is consistently slightly lower than the X-axis displacement, suggesting minor asymmetry in structural inertia distribution. Furthermore, the phase difference and time delay increase with rising frequency, reflecting the system's inherent high-frequency response lag. These observations provide critical reference data for the design and tuning of closed-loop compensators to achieve optimal dynamic performance and beam pointing stability.

5.3. Closed-Loop Stability Testing

To evaluate the control system's disturbance suppression capability under dynamic conditions, closed-loop stability tests were conducted. Experimental parameters matched those of the open-loop tests, maintaining identical frequency ranges and disturbance accelerations. During each test, peak spot displacement and steady-state error variations were recorded to assess the system's dynamic compensation performance.

As shown in Table 2, the peak displacements along the X- and Y-axes, steady-state errors, overshoot percentages, and rise times were systematically documented.

Table 2. Statistical Summary of Closed-Loop Stability Test Results.

Disturbance Frequency/ Hz	Disturbance Acceleration (g)	X-axis Peak Displacement (μm)	Y-axis Peak Displacement (μm)	Steady-State Error (μm)	Overshoot (%)	Rise time (ms)
50	0.1	0.9	0.8	0.12	3.6	0.9
100	0.1	1.1	1.0	0.15	4.2	1.0
200	0.3	2.0	1.8	0.20	5.1	1.3
300	0.3	2.7	2.5	0.26	6.4	1.4
400	0.5	3.3	3.1	0.33	7.2	1.5
500	0.5	4.1	3.8	0.38	7.9	1.7
600	0.5	5.2	4.9	0.44	8.6	1.9

Under closed-loop control, the peak spot offsets were reduced by approximately 70% on average compared to open-loop conditions, with steady-state errors maintained below 0.5 μm. Overshoot remained under 10% across all tested frequency bands, while rise times were consistently below 2 ms. The X- and Y-axis responses demonstrated strong consistency, validating the effectiveness of the inverse matrix decoupling algorithm. These results provide quantitative support for further optimization of control parameters and confirm the system's high-performance disturbance rejection capability.

5.4. Long-Term Stability and Repeatability Verification

To assess the system's long-term stability and repeatability under continuous operation, a 72-hour continuous run was conducted, complemented by 20 repeated spot positioning tests. The system remained in closed-loop control throughout, with spot positions sampled every 10 seconds to record displacement and ambient temperature variations over time.

As shown in Table 3, statistical processing of the collected data provided metrics for long-term drift and repeatability.

Table 3. Statistical Summary of Long-Term Operation and Repeatability Test Results.

Test Duration (h)	Ambient Temperature (°C)	X-axis Average Drift (μm)	Y-axis Average Drift (μm)	Maximum Offset (μm)	RMS Drift (μm)	Repeatability Error (μm)
0-6	25.1	0.38	0.35	0.62	0.21	0.19
6-12	25.3	0.41	0.37	0.67	0.23	0.22
12-24	25.2	0.45	0.43	0.73	0.26	0.25
24-36	25.0	0.49	0.46	0.81	0.29	0.27
36-48	24.9	0.52	0.49	0.85	0.32	0.28
48-60	25.2	0.54	0.51	0.89	0.34	0.29
60-72	25.3	0.57	0.53	0.93	0.35	0.31

Over the 72-hour continuous operation, the system exhibited a gradual but stable increase in drift, with average displacements on both X- and Y-axes remaining below 0.6 μm and RMS drift values under 0.35 μm. These results indicate that thermal effects and material stress have a controllable influence on pointing stability. Repeatability errors remained minimal, with consistent spot positioning differences observed across all 20 repeated tests. This confirms the system's high consistency, reliability, and suitability for prolonged precision applications.

6. Conclusions

This study presents a comprehensive investigation of a 4-axis PZT-driven laser beam pointing stabilization system, establishing a complete technical chain that encompasses

system architecture design, hardware configuration, dynamic modeling, algorithm development, and experimental verification. The implementation of dual-stage feedback control, combined with an inverse matrix decoupling algorithm, enables real-time compensation for multidimensional disturbances, effectively enhancing both dynamic response and long-term stability of the system.

Experimental results confirm that the proposed system achieves high control accuracy and excellent repeatability under complex disturbance conditions, with peak displacements significantly reduced in closed-loop operation and long-term drift maintained within sub-micron levels. The consistent X- and Y-axis responses further validate the robustness and reliability of the design, providing quantitative evidence for its practical application in precision optical systems.

Future work will focus on further expanding system capabilities, including the development of higher bandwidth control, advanced nonlinear compensation strategies, and optimized drive-channel matching. In addition, structural parameter refinement will be pursued to improve robustness under extreme environmental conditions, aiming to achieve highly reliable and adaptive beam stabilization performance for demanding optical applications.

References

1. L. Zhang, Y. Zhao, Y. Feng, L. Cao, J. Fu, J. Wang, and X. Li, "Effect of TaC on the microstructure and properties of WC-25Co cemented carbides additively manufactured by powder bed fusion-Laser beam," *International Journal of Refractory Metals and Hard Materials*, 2025.
2. J. Li, J. Wang, Z. Liu, X. Lyu, X. Liu, Z. Li, and X. Zhan, "Interplay of microstructure and mechanical properties in vacuum laser beam welded 50-mm-Thick titanium alloy Plates: Insights from molten pool flow simulation," *Optics & Laser Technology*, vol. 193, p. 114187, 2026. doi: 10.1016/j.optlastec.2025.114187
3. R. Wu, X. Wang, H. Fu, Z. Yang, Z. Wu, X. Li, and Z. Zhao, "Intrinsic quasi-isotropic tensile properties of powder bed fused-laser beam TiB2/AlMgScZr composites," *Journal of Alloys and Compounds*, 2025. doi: 10.1016/j.jallcom.2025.184411
4. N. Gupta, R. Johari, S. B. Bhardwaj, D. Bhardwaj, A. K. Alex, S. Shishodia, and N. Kohli, "Self-focusing, self-trapping and self-phase modulation of elliptical q-Gaussian laser beams in collisionless plasma," *Journal of Optics*, vol. 53, no. 1, pp. 181-196, 2024.
5. H. Kim, G. Park, and J. H. Lee, "Simulation and analysis of scattered light from laser beam dump inside the W divertor in KSTAR," *Fusion Engineering and Design*, vol. 222, p. 115484, 2026.